

# Bayesian Modelling of Pattern Formation from One Snapshot of Pattern

Natsuhiko Yoshinaga\*

*WPI - Advanced Institute for Materials Research,  
Tohoku University, Sendai 980-8577, Japan and  
MathAM-OIL, AIST, Sendai 980-8577, Japan*

Satoru Tokuda

*Research Institute for Information Technology, Kyushu University, Kasuga 816-8580, Japan and  
MathAM-OIL, AIST, Sendai 980-8577, Japan*

Partial differential equations (PDE) have been widely used to reproduce patterns in nature and to give insight into the mechanism underlying pattern formation. Although many PDE models have been proposed, they rely on the pre-request knowledge of physical laws and symmetries, and developing a model to reproduce a given desired pattern remains difficult. We propose a novel method, referred to as Bayesian modelling of PDE (BM-PDE), to estimate the best PDE for one snapshot of a target pattern under the stationary state. We show the order parameters extracting symmetries of a pattern together with Bayesian modelling successfully estimate parameters as well as the best model to make the target pattern. We apply BM-PDE to nontrivial patterns, such as quasi-crystals, a double gyroid and Frank Kasper structures. Our method works for noisy patterns and the pattern synthesised without the ground truth parameters, which are required for the application toward experimental data.

arXiv:2006.06125v1 [cond-mat.soft] 11 Jun 2020

---

\* corresponding authors: yoshinaga@tohoku.ac.jp

The design of structures of materials is one of the most important issues in various fields of physical science, as their structures are related to their physical properties. The structures are often characterised by periodic or quasi-periodic order. These ordered structures, which we call *pattern*, are ubiquitous in nature ranging from fluid convection[1] to microphase separation of block copolymers[2, 3] and atomic and molecular crystals[4, 5]. Surprisingly, the same pattern appears in different systems with completely different length scales[6]. Complex patterns such as quasi-crystal (QC), double gyroid (DG) and Frank Kasper (FK) phases appear not only in metallic alloy[7, 8] but also in soft materials such as block copolymers[2, 9], biomaterials[10], surfactants[11], liquid crystals[12] and colloidal assemblies[13]. Recent developments of imaging techniques give us various structural information, and thus it is desired to understand pattern formation and the design principle of a desired structure [14].

A continuum approach, such as the phase-field crystal (PFC) model based on the Landau theory on the phase transition, is particularly useful to give insight into a generic mechanism of symmetry selection in ordered structures[5, 6]. Using nonlinear partial differential equations (PDEs), the origins of pattern formation for various patterns have been investigated[5]. These studies have clarified generic pictures on a specific pattern under a specific model with parameters. Still, when encountering a new pattern, we need to choose a governing equation and tuning parameters. They require a sophisticated guess and trial-and-error. The typical situation is that we do not know a model to reproduce the pattern even though we know its properties such as the symmetry. Therefore, it is necessary to develop a method to estimate the best model for the target pattern independent from the model, rather than for data with ground truth.

Automatic discovery of a model equation is a recent key topic in data-driven science[15–17], and several methods have been proposed for PDEs of time-series data [18, 19]. Two major approaches are the regression and trajectory matching[20, 21]. Regression minimises the residue of a dynamical equation. This approach optimises parameters under the state noise added to the equation, but is weak under the measurement noise. Trajectory matching minimises the difference between measurement times series and solution of the candidate equation. It is robust under the measurement noise, but requires optimisation of its initial condition. These approaches cannot be applied to estimation for a stationary pattern, because it does not have information about the initial condition. We have to develop a method which is independent from the degeneracy of a pattern due to different initial conditions.

In this study, an inverse problem is formulated to reproduce a given snapshot of a pattern, after which we propose a method, referred to as Bayesian modelling of partial differential equations (BM-PDE), to identify the best PDE model and its parameters. We prepare the target pattern according to crystallographic symmetry, which is independent from any candidate models, and then perform estimation of the best model. We demonstrate it for complex patterns such as quasi-crystal, double gyroid and Frank Kasper A15 patterns.

## BAYESIAN MODELLING

We consider a pattern (or crystalline structures) expressed by the scalar density field  $\psi(\mathbf{x})$ . An example of a dodecagonal quasi-crystal is shown in Fig. 1(a,b). Higher density spots may be considered as a position of particles. We quantify the similarity between two patterns  $\psi_1$  and  $\psi_2$  by the distance between them defined as

$$E[\psi_1, \psi_2] = |\Psi[\psi_1] - \Psi[\psi_2]|^2. \quad (1)$$

Our target pattern is ordered and has many invariants; the pattern must be identified under change by translation and rotation, and also the pattern does not change by the action of symmetry group that the pattern has (see Fig. 1(a,b) and Supplementary Fig. S1 [22]). Here we introduce *order parameter*  $\Psi[\psi(\mathbf{x})]$ , which maps the pattern onto the feature space and eliminates the redundant information of the ordered pattern  $\psi(\mathbf{x})$  due to symmetry (see Fig. 1(c) and Methods).

We explore a model to reproduce a target pattern  $\psi^*(\mathbf{x})$  at the steady state  $\psi_s(\mathbf{x})$  of a model described by nonlinear partial differential equations  $\partial_t \psi(\mathbf{x}) = f[\psi(\mathbf{x})]$ . If the model and its parameters are ground truth, the target pattern satisfies,  $\partial_t \psi^*(\mathbf{x}) = f[\psi^*(\mathbf{x})] = 0$ . The basic structure of our estimation is schematically shown in Fig. 1(d). For a given model  $m_i$  and parameters  $\mu$  in a PDE, the stationary pattern is uniquely determined under each initial condition,  $\psi_0(\mathbf{x})$  (Fig. 1(c)). We treat an initial pattern as a latent variable that is marginalised using a random variable for the initial condition. This is because the obtained pattern may be translationally shifted or rotated by changing an initial pattern (see Fig 1(c)). The distance defined by equation (1) identify the patterns up to symmetry transformation thanks to the order parameter.

Our target pattern is *one* snapshot and has information only about the stationary state. This implies that when  $f[\psi^*(\mathbf{x})] = 0$  is a true model, we may have a series of *equally true* models such as  $f[\psi^*(\mathbf{x})]^2 = 0$ ,  $(f[\psi^*(\mathbf{x})] + 1) f[\psi^*(\mathbf{x})] = 0$  and so on. We therefore need to regularise the problem. This is realised by considering a family of PDE models based on physical properties. By selecting one model from the family, one can identify a relevant feature to reproduce the target pattern, and thus, can ensure interpretability. In the spirit of nonlinear dynamics of pattern formation,

the canonical form of the model should be described by the minimal number of terms and less spatial gradients. Hereafter, we construct a family of models based on this idea of parsimony.

We consider a model, called  $m \in M$ , expressed by a nonlinear partial differential equation (PDE) of the form

$$\partial_t \psi(\mathbf{x}) = \mathcal{L}_\mu^{(m)} \psi(\mathbf{x}) + \mathcal{N}[\psi(\mathbf{x})] \quad (2)$$

with a set of parameters  $\mu$ . The PDE is decomposed into two parts. The linear term is expressed by the linear operator,  $\mathcal{L}_\mu^{(m)}$ , acting on  $\psi(\mathbf{x})$  under a periodic domain. A possible extension of this approach will be discussed later. We make a family of models,  $M = \{m_i\}_{i \in [1, i_{\max}]}$ , by modifying the linear operator to have  $m_i$  peaks in its spectrum (see Methods and Fig. 1(e)). Our family of the models is designed to have a physical interpretation that the system has  $m_i$  length scales because peaks in the spectrum correspond to the number of length scales. Each length scale is characterised by its wavelength  $q_i$  and the value of its spectrum at the wavelength  $a_i$  (see Fig. 1(e)).

Our goal is to find the most probable model  $\hat{m}$  and parameters  $\hat{\mu}$  within the family for a given target pattern  $\psi^*(\mathbf{x})$ . To achieve this, we use the cost function  $E[\psi_s, \psi^*]$ , or called the energy, expressed by the order parameter  $\Psi$ , and compute the distance from the target pattern,  $\Psi^* = \Psi[\psi^*(\mathbf{x})]$ , to the numerically generated stationary pattern for each model and parameter set,  $\Psi[\psi_s(\mathbf{x})]$ . This form of energy resolves uncertainty originating from the measurement noise added in the target pattern. We carry out the Bayesian model selection using the log marginal likelihood, and the parameter estimation using the posterior distribution  $p(\mu|\Psi, m_i)$ , that is the probability of finding the parameters  $\mu$  under a given pattern and a model (see Fig. 1(d) and Methods).

## TWO-DIMENSIONAL QUASI-CRYSTAL WITH GROUND TRUTH

To give better insight into the BM-PDE, we first focus on an example of a two-dimensional quasi-crystal with 12-fold symmetry (dodecagonal quasi-crystal) shown in Fig. 1(a). This pattern has been studied using a model with two length scales[23]. The target pattern in this section is numerically produced with a set of parameters  $\mu^*$ . The two-length-scale model is used, that is,  $m^* = m_2$ .

For  $m = m_2$ , the energy  $E[\psi_s, \psi^*]$  decreases as the number of Monte Carlo steps increase, and the generated stationary patterns from equation (2) converge to quasi-crystals which are similar to the target pattern (Fig.2(b), see also Supplementary Fig.S2 [22]). The estimated parameters well agree to the parameters that we used to generate the target pattern (see Fig.2(d) and Supplementary Table.S1 [22]). The estimate length scale is  $q_1 = 0.52$  with the second length scale  $q_0 = 1$ . The ratio between them agrees to  $q_0/q_1 = 2 \cos(\pi/12) \approx 1.9319$ , which is the known value to generate this pattern[23]. The BM-PDE automatically estimates this ratio starting from prior distribution of the wavelength. The estimation also works for other parameters (Supplementary Table.S1 and Supplementary Fig.S2 [22]).

Using the estimated parameters, we may generate a pattern similar to the target pattern from uniform random initial density (see the inset of Fig.2(b)). To see the quality of the estimation, we measure the steady distribution of the energy. Figure 2(b) shows that there are two distinct states: one has higher energy  $E \gtrsim 10^2$  and the other has lower energy  $E \lesssim 10^2$ . The latter corresponds to quasi-crystal, whereas hexagonal patterns mainly dominate the former. The gap between the two states indicates that the quasi-crystal pattern requires a high resolution in the parameter search. The large step in the parameter space cannot find the optimal parameters because their range is narrow in the prior range of the parameters as in the inset of Fig.2(d). Therefore, the conventional gradient method with a fixed step size either cannot find the quasi-crystal when the step size is large, or impractical when it is small. The BM-PDE use hierarchical sampling, such as replica exchange Monte Carlo (REMC) [24, 25]. In this method, the knowledge of the step size corresponding to the inverse temperature  $\beta$  is not prerequisite for the parameter search.

The same algorithm is performed for the models with one length scale  $m = m_1$  and three length scale  $m = m_3$ . It is not surprising that the cost function  $E$  of the one-length-scale model is much higher than that of  $m_2$  because it cannot reproduce a quasi-crystal pattern (Fig. 2(a)). In fact, the model  $m = m_1$  with the estimated parameters produces hexagonal patterns rather than quasi-crystal ones. The three-length-scale model does reproduce a quasi-crystal pattern, which is comparable to the target pattern (Fig. 2(c)). However, our Bayesian estimation selects the two-length-scale model. Figure 2(e) demonstrates that the minimum free energy, that is, the marginal likelihood at the lowest temperature is lower for the two-length-scale model. Therefore, we estimate that this quasi-crystal pattern is described by the interaction of two modes with different length scale.

## TARGET PATTERNS WITHOUT GROUND TRUTH

The BM-PDE is not restricted to the estimation of the parameters that are used to generate the target pattern. We may synthesise a target pattern expressed analytically by properly superposing plane waves of the density field (see

Methods). This target pattern is independent of the models of equation (2), and is not necessarily a steady solution of one of them.

Using a two-dimensional dodecagonal quasi-crystal, we demonstrate that the BM-PDE successfully estimates the best model and approximated parameters for the target pattern without ground truth. The dodecagonal quasi-crystal is synthesised by the superposition of 12 plane waves (see Methods). The pattern is similar to numerically produced quasi-crystals used in the previous section (see Fig. 1(b) and Table 3(c)), but in the current case, there are no ground truth parameters and a true model. The target pattern can only approximately be accessed by one of the models in equation (2). In contrast with the numerically produced pattern, estimated parameters do not reproduce *exactly* the same pattern as the target pattern, and therefore the energy is relatively high (Supplementary Fig. S3 [22]). Nevertheless, both two-length-scale and three-length-scale models reproduce dodecagonal quasi-crystal patterns. The estimated parameters reproduce the inherent ratio of the length scales  $q_0/q_1 = 1.948 \approx 2 \cos(\pi/12)$ . The free energy indicates that the two length scale is favourable (Table. 3(c)).

We summarise the results of a variety of patterns in Table 3. For each target pattern, we can reproduce visually similar patterns, and the most probable number of length scales. In two-dimensional systems, stripe and hexagonal are the two most popular patterns under one length scale, that is, they are obtained from the conventional phase-field crystal model [26]. The free energy calculated in the BM-PDE indeed estimates that one length scale is favourable (Table 3(a,b)). The difference between stripe and hexagonal patterns appears in the mean density  $\bar{\psi}$ . A quadratic nonlinear term is necessary to reproduce hexagonal patterns, and this implies that it appears at  $|\bar{\psi}| \gg 0$  [26]. When  $\bar{\psi} \simeq 0$ , stripe patterns appear. The estimated values of the mean density are consistent with the results from forward-type studies [26]; we obtain  $\hat{\psi} \simeq -0.23$  and  $\hat{\psi} = -0.05$  for the hexagonal and stripe target patterns, respectively (see also Supplementary Fig. S6 [22]). The BM-PDE automatically estimates appropriate parameters from an artificially synthesised snapshot of the target pattern.

## DOUBLE GYROID AND FRANK KASPER PATTERNS

We discuss an application of the BM-PDE to non-trivial three-dimensional patterns. The target patterns are double gyroid (DG), shown in Fig. 3(d) and Frank Kasper (FK) A15, shown in Fig. 3(e). The DG structure has two separate domains each of which has degree-three vertices [10]. The DG structure was predicted theoretically [27, 28] and numerically [29], but mainly discussed in similar but different class of models of block copolymers [30]. FK A15 has been studied in metallic alloy and soft materials [9]. The self-consistent field theory, for example, designed to describe block copolymers, is capable of reproducing this pattern, but to our knowledge, this structure has not been reported within the framework of PFC.

Similar to the two-dimensional cases, we perform REMC to sample the best parameters and select the best model. In three dimensions, the order parameter may be defined similarly to that in two dimensions (see Methods). Structural candidates in three dimensions are far richer than two-dimensional patterns. In fact, during the sampling, cylindrical patterns with a hexagonal lattice, BCC, and other patterns appear. These patterns can be stable under a certain region of parameter space [31]. Despite these patterns being different from the target pattern, the BM-PDE can reproduce both the DG and FK A15 patterns both in the one- ( $m = m_1$ ) and two-length-scale ( $m = m_2$ ) models. The generated structure is the same as the target pattern, which is evident from the peaks in the Fourier space (Table 3(d,e) and Supplementary Sec. SVD [22]). The real space structures of the two patterns are overlapped by translation. The free energy in Fig. 3(d,e) shows that the target patterns of DG and FK A15 are expressed by the two length scale and one length scale, respectively.

The DG structure has two length scales with their ratio 1.15 (see Supplementary Sec. SVD [22]). In the one-length-scale model, by taking  $a_0 \gg 0$ , several modes with slightly different length scales may become unstable so that the double gyroid pattern is realised. In fact, it was discussed that DG appears not at  $a_0 = \epsilon \approx 0$  with the small number  $\epsilon$ , but at  $a_0 \gtrsim \mathcal{O}(1)$  [27, 28]. In addition, this pattern appears between the stripe patterns and cylindrical (hexagonal) patterns in the phase diagram, namely  $1 \gg |\bar{\psi}| \gtrsim 0$ . On the other hand, in the model of block copolymers, the FK A15 phase appears near BCC patterns in the phase diagram [9]. This suggests that  $|\bar{\psi}| \gg 0$  to obtain FK A15. The estimated mean density  $\bar{\psi}$  well agrees with this tendency. (Supplementary Figs. S12 and S13 [22]). The two models  $m_1$  and  $m_2$  have comparable probability for both patterns. The DG pattern chooses  $m_2$  possibly because  $m_2$  has a wider range of the spectrum amplitude in the phase diagram.

## ROBUSTNESS AGAINST NOISE

We hypothesise that the robust estimation of the model and parameters for the target pattern without ground truth originates from robustness against noise. To see this, we add Gaussian white noise in the target pattern and study

its effect on the estimation of the parameters. The dodecagonal quasi-crystal obtained from the numerical result of the two-length-scale model is used to produce the target pattern. Figure 4(a) shows that even when the amplitude of the noise is about 20% of the target pattern, the estimation of the parameter successfully works. Beyond the noise amplitude, the error of the estimated wavenumber becomes large, and the fraction of the patterns different from the target pattern increases. For the dodecagonal quasi-crystal, the wavenumber is required to be close to 0.51, and otherwise, the pattern cannot be generated because the mode coupling between two length scales does not occur.

We compare the BM-PDE with the standard regression methods in which parameters  $\mu$  are estimated by minimising the cost function  $\|\partial_t \psi - f(\psi; \mu)\|$  under an appropriate norm (see Supplementary Sec. SVI [22]). This method relies on the state noise added in the dynamical equation, and thus, does not give a good estimate for the measurement noise[20] (see Supplementary Sec.SVI [22]). In fact, Fig. 4(a) shows that the estimated wavenumber deviates from ground truth even under 0.1% noise amplitude.

In contrast with the noiseless target pattern, which has its free energy monotonically decreasing as the temperature decreases in Fig. 2(e), the free energy for the target pattern with noise has a minimum at the finite temperature as in Fig. 4(b). The minimum demonstrates the optimal temperature corresponding to the estimated noise amplitude to the target pattern[32]. The temperature at the free energy minimum increases as the amplitude of noise increases. At the large noise amplitude  $\gtrsim 30\%$ , the minimum temperature reaches a comparable value with the energy at the gap between two structures in Fig. 2(b): quasi-crystal and hexagonal patterns. Thus, dodecagonal quasi-crystals can no longer be reproduced. Interestingly, the free energy minimum is also observed for the target pattern synthesised by the function. In this case, there is no ground truth parameter that reproduces exactly the same pattern as the target pattern. The optimal temperature at the free energy minimum describes the deviation of the target pattern from the patterns that the models can reach. Without the Bayesian inference, we cannot successfully estimate the uncertainty, which plays a similar role to noise.

## DISCUSSIONS AND CONCLUSION

In summary, we propose the inverse problem of equation discovery for a stationary pattern. We demonstrate that the BM-PDE can estimate not only the model that reproduces a target pattern, but also estimates the best model for the pattern. The success of our approach relies on the order parameters, the Bayesian inference, and a family of models. The order parameters can extract symmetries of the pattern, and identify the two patterns that are generated with the same parameters but the different initial conditions. In order to perform statistical inference, we use REMC, which efficiently compute a posterior probability distribution. This enables us to evaluate the marginal likelihood of the model, and to select the best model among the different number of length scales.

The BM-PDE not only works for a numerically produced pattern, which has ground truth of parameters, but also for an analytically synthesised pattern. In the latter case, our family of models does not include ground truth. Nevertheless, the BM-PDE successfully estimate the best model and parameters among the family. Because the BM-PDE estimates the optimal noise amplitude, the method is robust against noise and also quantify the uncertainty of the estimation. We expect this method can also be applied to images of experimental results.

The BM-PDE may be extended to other families of models. In order to make quasi-crystals, at least two methods are known other than the multiple length scales: the multiple species of density field[33] and anisotropic interactions[34, 35] (see Supplementary Sec.SIA [22]). Our approach may be applied to those families of models.

## METHODS

### *Bayesian modelling of partial differential equations (BM-PDE)*

The main framework of BM-PDE consists of three parts: a family of models, order parameter, and statistical inference. Here, we summarise their basic steps. The detailed formula is given in Supplementary Information[22].

### *Family of models*

We consider a family of models based on the phase-field crystal model of equation (2). In this work, the nonlinear term is fixed by  $\mathcal{N}[\psi] = \Delta\psi^3$ , for simplicity. Each model in the family has a different functional form of the linear operator  $\mathcal{L}_k$  in the Fourier space. In the model with  $m$  length scales, it is expressed as

$$\mathcal{L}_k = a_0 S_0(k) + a_1 S_1(k) + \dots + a_{m-1} S_{m-1}(k) + s_0 k^2 (q_0^2 - k^2)^2 (q_1^2 - k^2)^2 \dots (q_{m-1}^2 - k^2)^2. \quad (3)$$

The function  $S_i(k)$  for  $i \in [0, m-1]$  is chosen so that the coefficient  $a_i$  corresponds to the peak as a function of  $k$  of  $\mathcal{L}_k$  at  $k = 1_i$  (see Fig. 1(e)). This implies that we impose the length scale  $2\pi/q_i$ . The detailed form of  $S_i(k)$  is shown in Supplementary Information[22]. The parameter  $s_0$  describes sharpness of the peaks. To make the spectrum sharp enough, we chose the parameter to be  $s_0 = 100$  for the one-length and two-length models, and  $s_0 = 2000$  for the three-length model. Both  $a_i$  and  $q_i$  are chosen as parameters to be optimised. We have other parameters such as the system size  $L$  in each direction and the mean density of a pattern  $\bar{\psi}$ . In this study, we use the periodic boundary condition. A set of parameters is thus  $\mu = \{L_\alpha, \bar{\psi}, a_0, q_0, \dots, a_{l-1}, q_{l-1}\}$  with  $\alpha \in [1, \dots, d]$  in space dimension  $d$ .

In order to make a pattern, higher-order spatial derivatives are necessary. Polynomial expansion in terms of the wavenumber  $k$  instead of equation (3) may be available to make several length scales (see Fig. 1(e)). Nevertheless, it suffers from the large value of the coefficient of each order in the polynomials because we may not use prior distribution to confine the parameter space (see Supplementary Sec. SIII B [22]).

### *Order parameter*

To assure translational invariance, we use a spectrum of the Fourier transform of the pattern, and expand it by the basis functions, each of which express certain point group symmetries. In two dimensions, the basis functions reflect  $n$ -fold rotational symmetry, as shown in Fig. 1(b), whereas in three dimensions, spherical harmonics expansion is used. Projection of the Fourier spectrum of the pattern onto the basis function is given by  $A_{l,\pm}$  in two dimensions, and  $A_{lm}$  in three dimensions.

The order parameter is a rotational invariant form of the quantity  $A_{lm}$  with  $l \in [0, l_0]$  and  $m \in \{\pm 1\}$  in two dimensions and  $m \in [-l, l]$  in three dimensions. In two dimensions,  $A_{l,\pm 1}$  is described by

$$A_{l,\pm 1}[\psi] = \int |\psi(\mathbf{k})| \begin{pmatrix} \cos l\theta_k \\ \sin l\theta_k \end{pmatrix} d\mathbf{k}^2 \quad (4)$$

where  $+1$  ( $-1$ ) corresponds to  $\cos l\theta_k$  ( $\sin l\theta_k$ ), respectively, and  $\theta_k$  is a polar angle in the Fourier space. We denote  $A_{l,\pm}$  in the vector form as  $\mathbf{A}_l = (A_{l,+}, A_{l,-})$ . The maximum mode is denoted by  $l_0$ . In three dimensions,  $A_{lm}$  is given by

$$A_{lm}[\psi] = \int |\psi(\mathbf{k})| Y_l^m(\theta_k, \varphi_k) d\mathbf{k}^3 \quad (5)$$

with spherical harmonics  $Y_l^m(\theta_k, \varphi_k)$  in the spherical coordinates of the Fourier space  $(k, \theta_k, \varphi_k)$ . Note that  $m$  in the superscript of  $Y_l^m(\theta_k, \varphi_k)$  and subscript of  $A_{lm}$  should not be confused by  $m$  describing a model in  $M$ . We define the order parameter  $\Psi[\psi(\mathbf{x})]$  by a rotationally invariant form of the coefficients,  $A_{l,\pm}$  or  $A_{lm}$  (see Supplementary Sec. SIII [22]).

$$\Psi_l = \|\mathbf{A}_l\| \equiv \sqrt{A_{l,+}^2 + A_{l,-}^2} \quad (6)$$

in two dimensions, and

$$\Psi_l = \|A_{lm}\| \equiv \sqrt{\frac{4\pi}{2l+1}} \sqrt{\sum_{m=-l}^l (-1)^m A_{l,m} A_{l,-m}} \quad (7)$$

in three dimensions.

### Statistical inference

To estimate the best parameter set  $\mu$  and the best model  $m$ , as well as their uncertainty, we consider statistical inference. Our purpose is not to estimate specific initial states  $\psi_0$  for the target pattern  $\psi^*$ , but to estimate the best model that could generate patterns similar to  $\psi^*$  independent of the initial state. Therefore, our best parameter set  $\hat{\mu}$  is defined by the mean of the marginal probability distribution (see also Supplementary Sec. SIV [22])

$$p(\mu | \Psi^*, \beta, m) = \int p(\psi_0) p(\mu | \Psi^*, \psi_0, \beta, m) d\psi_0. \quad (8)$$

Following Bayes' theorem, the posterior distribution is given by

$$p(\mu | \Psi^*, \psi_0, \beta, m) = \frac{p(\Psi^* | \psi_0, \mu, \beta, m) p(\mu | m)}{p(\Psi^* | m, \beta)}. \quad (9)$$

The likelihood is represented by  $p(\Psi^* | \mu, m, \beta) \propto e^{-\beta E[\psi, \psi^]}$ , where the inverse temperature  $\beta$  is associated with variance of the observation noise. This likelihood implies that the error in the measurement is given by  $\Psi^* = \Psi + \xi$  with the Gaussian noise  $\xi$  with zero mean and its variance  $\beta^{-1}$ . The prior distributions  $p(\psi_0)$  and  $p(\mu | m)$  are defined by the uniform distribution. The normalisation factor  $p(\Psi^* | \beta, m)$ , or the log marginal likelihood (free energy)  $F(\beta, m) \equiv -\log p(\Psi^* | \beta, m)$ , is one of the criteria of model selection and hyperparameter estimation [36, 37]. Our best model  $m$  and inverse temperature  $\beta$  are both determined by maximising  $p(\Psi^* | \beta, m)$ , or equivalently, minimising  $F(\beta, m)$  [32] (see also Supplementary Sec. SIV [22]).

The realisation of  $p(\mu | \Psi^*, \psi_0, m, \beta)$  is carried out by Monte Carlo (MC) sampling in the parameter space. For each point in the parameter space, we compute a stationary pattern  $\psi_s$  in the model of equation (2) under the randomly obtained  $\psi_0$ , and then move in the parameter space stochastically according to the Metropolis criterion defined by the cost function (energy)  $E[\psi, \psi^*]$  and inverse temperature  $\beta$ . We use the REMC method [24, 25] with different inverse temperatures  $\beta$  in parallel. The REMC is an efficient method for the estimation of the optimal variance  $\hat{\beta}^{-1}$  of the observation noise because the method enables us to sample parameters simultaneously under various  $\beta$ . The method also makes an efficient sampling to avoid a local trap in the parameter space. Bridge sampling [38, 39] is used to calculate  $F(m, \beta)$  for each  $m$ . The error bars of  $F(m, \beta)$  are calculated by the bootstrap resampling [40].

### Target Pattern

A target pattern  $\psi^*(\mathbf{x})$  is prepared in two ways. One is a numerical solution of equation (2) for given parameters under a given model. The resulting pattern is numerically transformed into the Fourier space, and then the order parameter  $\Psi_l^*$  is calculated.

The second way is completely independent of the models. The target pattern is expressed as a density field  $\psi^*(\mathbf{x})$  that is a superposition of the cosine function. The simplest case is a stripe pattern, which is described only by one wave in one direction in a two-dimensional space. Similarly, a hexagonal pattern is expressed by two-dimensional waves in three directions. The target pattern is expressed as

$$\psi^*(\mathbf{x}) = \sum_i b_i \cos(\mathbf{q}_i^* \cdot \mathbf{x}) \quad (10)$$

where the wave vectors  $\mathbf{q}_i^*$  are chosen at the position appropriate to express symmetries of the target pattern. The amplitude of each mode  $b_i$  is also chosen properly. We numerically make the Fourier transform of equation (10) to obtain  $\hat{\psi}^*(\mathbf{k}) = \mathcal{F}[\psi^*(\mathbf{x})]$  and calculate the Fourier spectrum  $|\hat{\psi}^*(\mathbf{k})|$  from which we obtain the order parameter. The Fourier transform of equation (10) defined in the infinite domain is expressed by superposition of the delta function at the position of  $\mathbf{q}_i^*$ . Nevertheless, the numerical Fourier transform in the bounded domain results in peaks smeared around  $\mathbf{q}_i^*$ . To remove the artefact, we set  $|\psi^*(\mathbf{k})| = 0$  except for the region  $|\psi^*(\mathbf{k})| > \alpha \max |\psi^*(\mathbf{k})|$ . Here, the value of  $\alpha$  is chosen so that the peaks of the minimal height are left. We choose  $\alpha = 0.6$  for the two-dimensional target patterns, whereas  $\alpha = 0.01$  for the three-dimensional target patterns.

The dodecagonal quasi-crystal pattern is synthesised by  $\psi = \sum_{i=1}^{12} \cos(\mathbf{q}_i^* \cdot \mathbf{x})$  in which the wave vectors  $\mathbf{q}_i^*$  are chosen at the position of the vertices of the hexagon with a radius  $|\mathbf{q}_1^*| = 2\pi/\sqrt{2 + \sqrt{3}}$  and the hexagon with a radius  $|\mathbf{q}_2^*| = 2\pi$  rotated by  $\pi/12$ . The DG pattern is expressed by 24 wave vectors of  $\mathbf{q}^* = (\pm 2, \pm 1, \pm 1)$  and 12 wave

vectors of  $\mathbf{q}^* = (\pm 2, \pm 2, 0)$  with their permutation along the  $x, y, z$  directions[41, 42]. The amplitude of the latter wave vector is  $\sqrt{8/6} \simeq 1.15$  times longer than the former waves. The FKA15 pattern is expressed by 24 wave vectors  $\mathbf{q}^* = (\pm 2, \pm 1, 0)$ , 24 wave vectors  $\mathbf{q}^* = (\pm 2, \pm 1, \pm 1)$ , 6 wave vectors of  $\mathbf{q}^* = (\pm 2, 0, 0)$  with their permutation along the  $x, y, z$  directions[43].

### *Numerical simulations*

Numerical simulations of the PDEs are performed using the pseudo-spectral method in which the linear terms are computed in the Fourier space, and the nonlinear terms are computed in real space. Since our PDEs contain higher-order derivatives, we use the operator-splitting method[44, 45]. Both real and Fourier spaces are discretised into  $N^d$  meshes in  $d$ -dimensional space. Instead of changing the system size  $L_i$  in each dimension  $i \in [1, d]$  under the periodic domain, we change the mesh size  $dx_i$  so that the system size becomes  $L_i = (N - 1)dx_i$ .

The number of mesh points is fixed to be  $N = 128$  in two dimensions and  $N = 32$  in three dimensions. The larger  $N$  is better in terms of accuracy, but computational time is scaled roughly as  $\mathcal{O}(N^d)$ . In REMC, we need to simulate it in  $N_{\text{rep}}$  replicas, and therefore, the choice of  $N$  is made by the balance between accuracy and realistic computational time. In addition, the larger system size suffers from longer relaxation time and a higher probability that topological defects such that dislocations and disclinations appear. We set the total number of steps to be  $10^5$  with a time step  $dt = 0.01$ . We conformed this is enough to obtain the stationary patterns studied in this work, but may be changed depending on the pattern of interest. Note that statistical inference in this study is completely independent from the algorithm of numerical simulations solving a PDE. Efficient algorithm would improve the performance of estimation, and one may replace the numerical scheme suit for one's purpose.



## CODE AVAILABILITY

All codes used in this work are written in MATLAB and freely available from the corresponding author upon a request.

## DATA AVAILABILITY

The data that support the findings of this study are available from the corresponding author on reasonable request.

## ACKNOWLEDGMENTS

The authors are grateful to Edgar Knobloch, Yasumasa Nishiura, An-Chuang Shi, and Philippe Marcq for helpful discussions. The authors acknowledge the support by JSPS KAKENHI grant numbers 17K05605, 20H05259, and 20K03874 to N.Y. and 20K19889 to S.T. Numerical simulations in this work were carried out in part by AI Bridging Cloud Infrastructure (ABCI) at National Institute of Advanced Industrial Science and Technology (AIST).

## AUTHOR CONTRIBUTION

N.Y. and S.T. conceived the research. N.Y. carried out simulations. N.Y. and S.T. analysed the results. N.Y. and S.T. wrote the manuscript.

## MATERIALS & CORRESPONDENCE

Supplementary information accompanies this paper on “<http://www.wpi-aimr.tohoku.ac.jp/~yoshinaga/publication/Supplement20200522.pdf>”. Correspondence and requests for materials should be addressed to N.Y.

## COMPETING INTERESTS STATEMENT

The authors declare no competing financial interests.

- 
- [1] Swift, J. & Hohenberg, P. C. Hydrodynamic fluctuations at the convective instability. *Phys. Rev. A* **15**, 319–328 (1977).
  - [2] Bates, F. S. & Fredrickson, G. H. Block copolymer thermodynamics: Theory and experiment. *Annu. Rev. Phys. Chem.* **41**, 525–557 (1990).
  - [3] Harrison, C. *et al.* Mechanisms of ordering in striped patterns. *Science* **290**, 1558–1560 (2000).
  - [4] Elder, K. R., Katakowski, M., Haataja, M. & Grant, M. Modeling elasticity in crystal growth. *Phys. Rev. Lett.* **88**, 245701 (2002).
  - [5] Provatas, N. & Elder, K. *Phase-field methods in materials science and engineering* (John Wiley & Sons, 2011).
  - [6] Cross, M. & Hohenberg, P. Pattern formation outside of equilibrium. *Rev. Mod. Phys.* **65**, 851–1112 (1993).
  - [7] Frank, F. C. & Kasper, J. S. Complex alloy structures regarded as sphere packings. II. Analysis and classification of representative structures. *Acta Crystallographica* **12**, 483–499 (1959).
  - [8] Shechtman, D., Blech, I., Gratias, D. & Cahn, J. W. Metallic phase with long-range orientational order and no translational symmetry. *Phys. Rev. Lett.* **53**, 1951–1953 (1984).
  - [9] Bates, M. W. *et al.* Stability of the a15 phase in diblock copolymer melts. *Proc. Nat. Acad. Sci. USA* **116**, 13194–13199 (2019).
  - [10] Scherer, M. R. J. *Gyroid and Gyroid-Like Surfaces*, 7–19 (Springer International Publishing, Heidelberg, 2013).
  - [11] Yue, K. *et al.* Geometry induced sequence of nanoscale frank-kasper and quasicrystal mesophases in giant surfactants. *Proc. Nat. Acad. Sci. USA* **113**, 14195–14200 (2016).
  - [12] Zeng, X. *et al.* Supramolecular dendritic liquid quasicrystals. *Nature* **428**, 157–160 (2004).
  - [13] Hynninen, A.-P., Thijssen, J. H. J., Vermolen, E. C. M., Dijkstra, M. & van Blaaderen, A. Self-assembly route for photonic crystals with a bandgap in the visible region. *Nat. Mater.* **6**, 202–205 (2007).

- [14] Kalinin, S. V., Sumpster, B. G. & Archibald, R. K. Big-deep-smart data in imaging for guiding materials design. *Nat. Mater.* **14**, 973 (2015).
- [15] Daniels, B. C. & Nemenman, I. Automated adaptive inference of phenomenological dynamical models. *Nat. Commun.* **6**, 8133– (2015).
- [16] Brunton, S. L., Proctor, J. L. & Kutz, J. N. Discovering governing equations from data by sparse identification of nonlinear dynamical systems. *Proc. Nat. Acad. Sci. USA* **113**, 3932–3937 (2016).
- [17] Brunton, S. L. & Kutz, J. N. *Data-driven Science and Engineering: Machine Learning, Dynamical Systems, and Control* (Cambridge University Press, 2019).
- [18] Rudy, S. H., Brunton, S. L., Proctor, J. L. & Kutz, J. N. Data-driven discovery of partial differential equations. *Sci. Adv.* **3**, e1602614 (2017).
- [19] Zhao, H., Storey, B. D., Braatz, R. D. & Bazant, M. Z. Learning the physics of pattern formation from images. *Phys. Rev. Lett.* **124**, 060201 (2020).
- [20] Voss, H. U., Timmer, J. & Kurths, J. Nonlinear dynamical system identification from uncertain and indirect measurements. *Int. J. Bifurcat. Chaos* **14**, 1905–1933 (2004).
- [21] Müller, T. G. & Timmer, J. Parameter identification techniques for partial differential equations. *Int. J. Bifurcat. Chaos* **14**, 2053–2060 (2004).
- [22] Supplementary Information is available on '<http://www.wpi-aimr.tohoku.ac.jp/~yoshinaga/publication/Supplement20200522.pdf>'.
- [23] Lifshitz, R. & Petrich, D. M. Theoretical model for faraday waves with multiple-frequency forcing. *Phys. Rev. Lett.* **79**, 1261–1264 (1997).
- [24] Geyer, C. J. Markov chain monte carlo maximumlikelihood. *Computing science and statistics: Proceedings of the 23rd Symposium on the Interface, American Statistical Association* **156** (1991).
- [25] Hukushima, K. & Nemoto, K. Exchange monte carlo method and application to spin glass simulations. *J. Phys. Soc. Japan* **65**, 1604–1608 (1996).
- [26] Elder, K. R. & Grant, M. Modeling elastic and plastic deformations in nonequilibrium processing using phase field crystals. *Phys. Rev. E* **70**, 051605 (2004).
- [27] Podneps, V. E. & Hamley, I. W. Landau- brazovskii theory for the ia3d structure. *J. Exp. Theor. Phys. Lett.* **64**, 617–624 (1996).
- [28] Shi, A.-C. Nature of anisotropic fluctuation modes in ordered systems. *J. Phys. Cond. Mat.* **11**, 10183 (1999).
- [29] Zhang, P. & Zhang, X. An efficient numerical method of landau-brazovskii model. *J. Comp. Phys.* **227**, 5859 – 5870 (2008).
- [30] Nonomura, M. & Ohta, T. Kinetics of morphological transitions between mesophases. *J. Phys. Cond. Mat.* **13**, 9089–9112 (2001).
- [31] Jaatinen, A. & Ala-Nissila, T. Extended phase diagram of the three-dimensional phase field crystal model. *J. Phys. Cond. Mat.* **22**, 205402 (2010).
- [32] Tokuda, S., Nagata, K. & Okada, M. Simultaneous estimation of noise variance and number of peaks in bayesian spectral deconvolution. *J. Phys. Soc. Japan* **86**, 024001 (2017).
- [33] Mermin, N. & Troian, S. M. Mean-field theory of quasicrystalline order. *Phys. Rev. Lett.* **54**, 1524 (1985).
- [34] Kats, E., Lebedev, V. & Muratov, A. Weak crystallization theory. *Phys. Rep.* **228**, 1–91 (1993).
- [35] Müller, H. W. Model equations for two-dimensional quasipatterns. *Phys. Rev. E* **49**, 1273–1277 (1994).
- [36] MacKay, D. J. Bayesian interpolation. *Neural comput.* **4**, 415–447 (1992).
- [37] Bishop, C. M. *Pattern recognition and machine learning I*, vol. 1 (springer New York, 2006).
- [38] Meng, X.-L. & Wong, W. H. Simulating ratios of normalizing constants via a simple identity: a theoretical exploration. *Statistica Sinica* 831–860 (1996).
- [39] Gelman, A. & Meng, X.-L. Simulating normalizing constants: From importance sampling to bridge sampling to path sampling. *Statistical science* 163–185 (1998).
- [40] Efron, B. Bootstrap methods: another look at the jackknife. In *Breakthroughs in statistics*, 569–593 (Springer, 1992).
- [41] von Schnering, H. G. & Nesper, R. Nodal surfaces of fourier series: Fundamental invariants of structured matter. *Z. Phys. B* **83**, 407–412 (1991).
- [42] Yamada, K., Nonomura, M. & Ohta, T. Kinetics of morphological transitions in microphase-separated diblock copolymers. *Macromolecules* **37**, 5762–5777 (2004).
- [43] Impéror-Clerc, M. Three-dimensional periodic complex structures in soft matter: investigation using scattering methods. *Interface focus* **2**, 589–601 (2012).
- [44] Cox, S. & Matthews, P. Exponential time differencing for stiff systems. *J. Comp. Phys.* **176**, 430–455 (2002).
- [45] Aranson, I. S. (ed.) *Physical Models of Cell Motility* (Springer, Cham, 2015).

## FIGURES AND TABLES

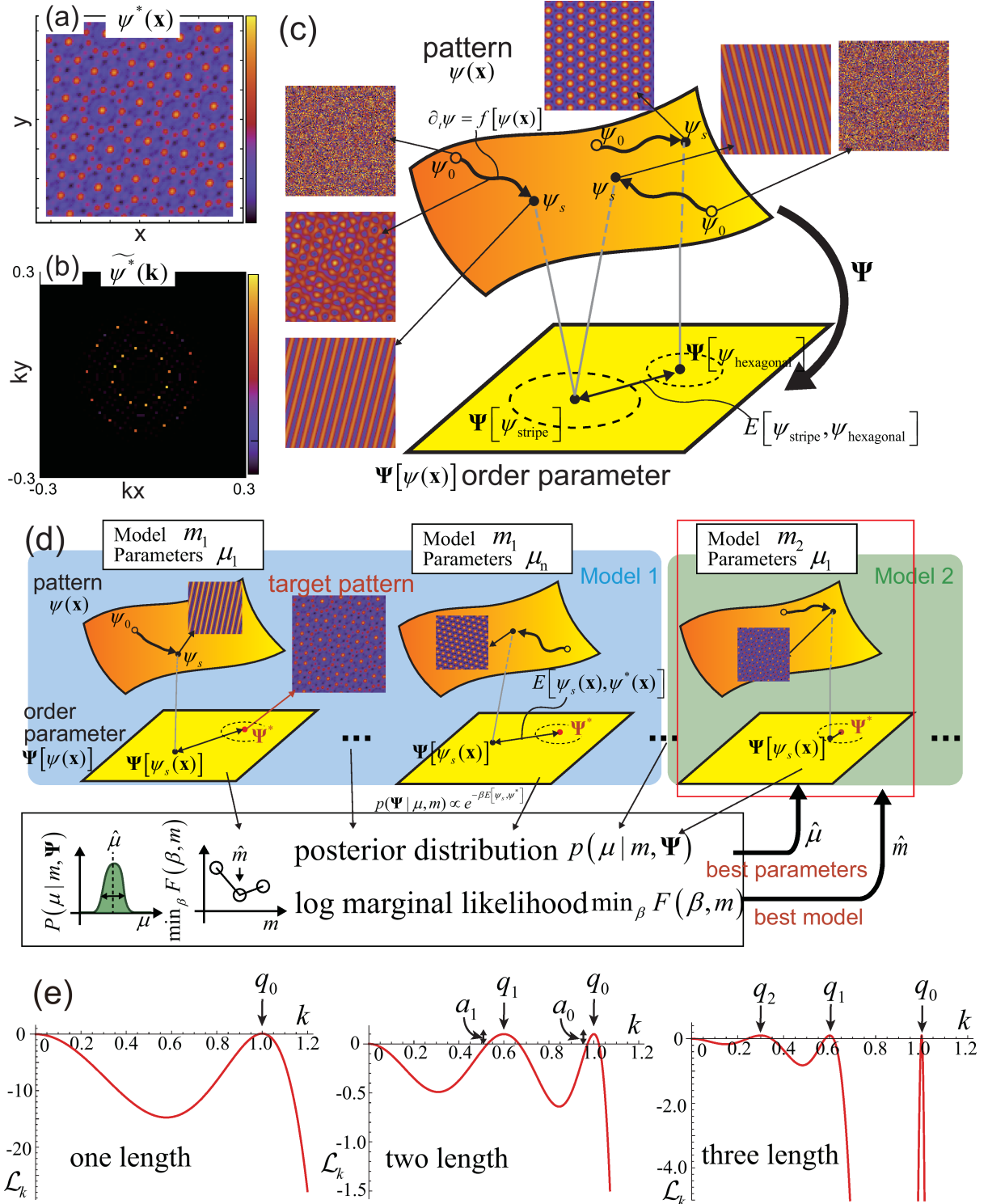


FIG. 1. Schematic illustration of Bayesian modelling of partial differential equations (BM-PDE). (a,b) The example of the target pattern of a dodecagonal quasi-crystal produced from a numerical result (a), and its Fourier transform (b). The colour bar indicates  $[-1.5, 3.5]$  in (a) and  $[0, 3000]$  in (b). (c) The space of patterns  $\psi(\mathbf{x})$  and order parameters  $\Psi[\psi(\mathbf{x})]$ . The PDE is solved with the initial condition  $\psi_0$  taken from random variables. For each trajectory, the translational position and orientation of the pattern  $\psi_s$  would change even under exactly the same parameters and the same model. The order parameter identifies the two patterns by extracting symmetries of the pattern. The distance between two patterns is quantified by  $E$ . (d) For each set of parameters, there is a stationary pattern  $\psi_s$ . The cost function  $E[\psi_s^*, \psi_s]$  (energy) is calculated from the order parameters of the target and generated patterns. From the posterior distribution, the best parameters and their errors are estimated. The distribution of the cost function gives the log marginal likelihood of the model from which the selection of models can be made. (e) Linear stability of multi-length-scale phase field crystal equations. The plots show eigenvalues as a function of the wavenumber. Positive eigenvalues imply the uniform state is unstable.

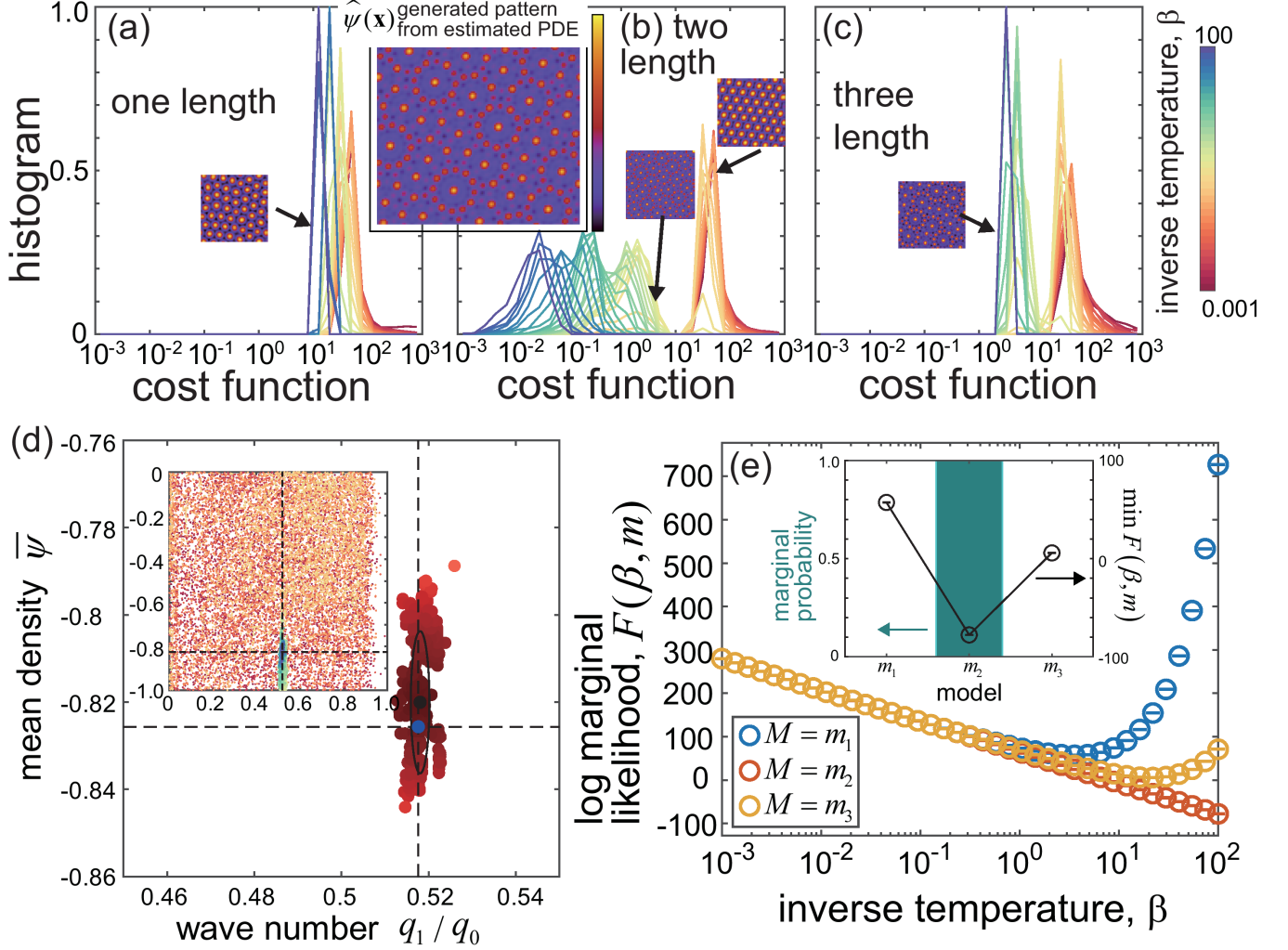


FIG. 2. Model selection and parameter estimation for the target pattern of two-dimensional quasi-crystal pattern with 12-fold (dodecagonal) symmetry. (a-c) The histograms of the cost function,  $E[\psi^*, \psi_s]$ , during the sampling. The horizontal axis is shown in the logarithmic scale. The generated pattern from the estimated PDE is shown in the insets. Typical patterns at each energy range are also shown in the insets with arrows. (d) The estimated parameters in the space spanned by  $q_1$  and  $\bar{\psi}$ . The colour indicates histogram where darker red corresponds to higher probability. The mean and standard deviation of the estimated parameters are shown in the black point and the black line, respectively. The ground truth parameter values are shown in dashed lines and the blue point. The inset shows the same plot under various  $\beta$  in REMC in the range of parameters used for the prior distribution. The same colour code as (a-c) is used. (e) Model selection is made by the log marginal likelihood (free energy) calculated from the steady state energy distribution for  $m_1$  (a),  $m_2$  (b), and  $m_3$  (c). The inset shows the probability of each model marginalised for all  $\beta$ . The minimal free energy of each model is also shown with error bars, which overlap with the points.

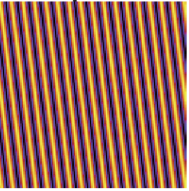
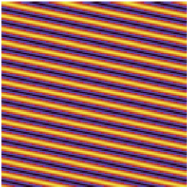
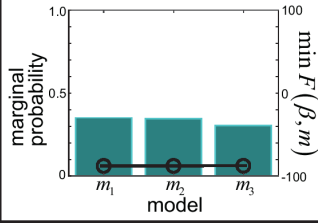
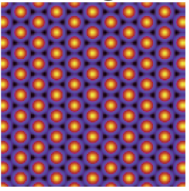
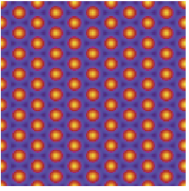
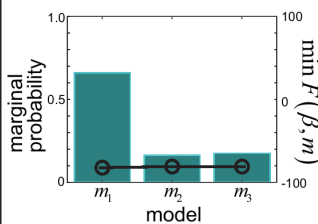
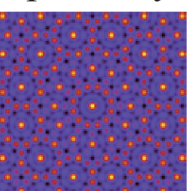
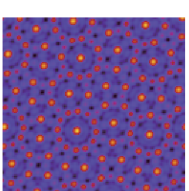
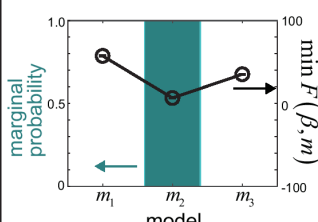
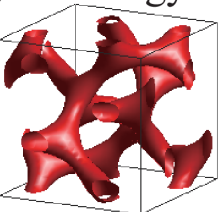
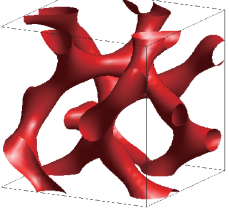
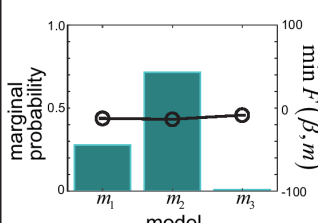
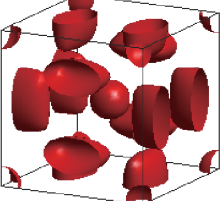
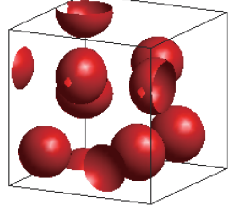
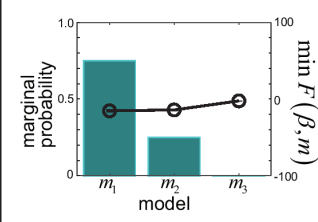
target pattern	generated pattern from estimated parameters	length scale estimation from log marginal likelihood	estimated parameters
(a) stripe 			one length scale $\bar{\psi} = -0.0471 \pm 0.0351$ $q_0 = 0.704 \pm 0.103$
(b) hexagonal 			one length scale $\bar{\psi} = -0.226 \pm 0.054$ $q_0 = 0.503 \pm 0.004$
(c) quasi-crystal 			two length scale $\bar{\psi} = -0.748 \pm 0.019$ $q_0 / q_1 = 0.514 \pm 0.004$
(d) double gyroid 			two length scale $\bar{\psi} = -0.090 \pm 0.027$ $q_1 / q_0 = 0.419 \pm 0.0187$
(e) Frank Kasper A15 			one length scale $\bar{\psi} = -0.365 \pm 0.024$ $q_0 = 0.416 \pm 0.015$

FIG. 3. Summary of target and estimated patterns for stripe (a), hexagonal (b), 12-fold symmetric quasi-crystal (c), double gyroid (d), and Frank Kasper A15 (e). For each pattern, the free energy is evaluated for a model with one-, two-, and three-length scales. The best model is selected from minimum free energy. The model uncertainty is quantified by the marginal probability of each model obtained from the free energy marginalised for all temperatures.

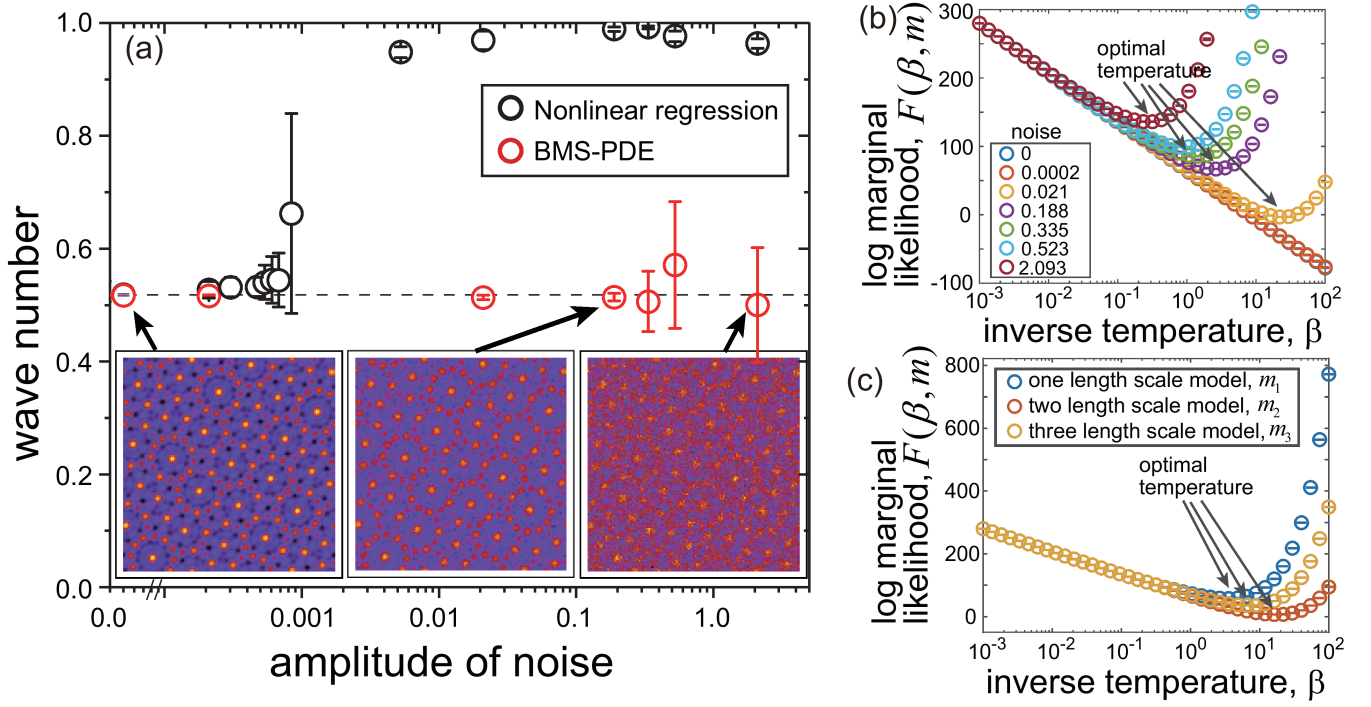


FIG. 4. (a) Estimated wavenumbers for numerically generated quasi-crystal by BM-PDE equation (1) (red points) and conventional regression method (black points) under Gaussian white noise added on the target pattern (see equation (S60) in Supplementary Information). Noise amplitude with respect to the variance of the noiseless pattern is defined as  $\sigma^2/\text{Var}[\psi^*]$  where  $\sigma^2$  is the variance of added noise. The horizontal dashed line indicates the ground truth of the wavenumber  $q_1 = 0.51764$ . The target patterns under the different noise amplitude is shown in the insets. (b) The free energy at each inverse temperature  $\beta$  for the target pattern generated by the numerical simulation with noise corresponding to (a). The minimums of the free energy are shown by arrows. (c) The free energy at each inverse temperature  $\beta$  in REMC under the models  $m_1$ ,  $m_2$ , and  $m_3$  for the target pattern synthesised by the function.